universe

IMPACT FACTOR 2.6

CITESCORE 5.2

Article

Correlating the $0\nu\beta\beta$-Decay Amplitudes of ^{136}Xe with the Ordinary Muon Capture (OMC) Rates of ^{136}Ba

Aagrah Agnihotri, Vikas Kumar and Jouni Suhonen

Special Issue

Exploring Double Beta Decay: Probing Fundamental Properties of Neutrinos and Beyond

Edited by

Prof. Dr. Rita Bernabei

MDPI

https://doi.org/10.3390/universe11050138

universe

MDPI

Article

Correlating the $0\nu\beta\beta$-Decay Amplitudes of ^{136}Xe with the Ordinary Muon Capture (OMC) Rates of ^{136}Ba

Aagrah Agnihotri [1,2,*], Vikas Kumar [1,3] and Jouni Suhonen [1,2]

[1] Department of Physics, University of Jyväskylä, P.O. Box 35 (YFL), 40014 Jyväskylä, Finland; vikas.v.kumar@jyu.fi or vikasphysics@bhu.ac.in (V.K.); jouni.t.suhonen@jyu.fi (J.S.)
[2] International Centre for Advanced Training and Research in Physics (CIFRA), P.O. Box MG12, 077125 Bucharest, Romania
[3] Banaras Hindu University, Varanasi 221005, Uttar Pradesh, India
* Correspondence: aagrah.a.agnihotri@jyu.fi

Abstract: The potential correlation between the ordinary muon capture (OMC) on ^{136}Ba and $0\nu\beta\beta$ decay of ^{136}Xe is explored. For this, we compute $0\nu\beta\beta$-decay amplitudes for intermediate states in ^{136}Cs below 1 MeV of excitation and for angular-momentum values $J \leq 5$ by using the proton–neutron quasiparticle random-phase approximation (pnQRPA) and nuclear shell model (NSM). We compare these amplitudes with the corresponding OMC rates, computed in a previous Universe article (Universe 2023, 9, 270) for the same energy and angular-momentum ranges. The obtained results suggest that an extension of the present analysis to a wider energy and angular-momentum region could be highly beneficial for probing the $0\nu\beta\beta$-decay nuclear matrix elements using experimental data on OMC rates to intermediate states of $0\nu\beta\beta$ decays.

Keywords: double beta decay of Xe-136; nuclear matrix elements; muon capture on Ba-136; muon-capture rates

Academic Editors: Rita Bernabei and Andreas Aste

Received: 19 March 2025
Revised: 15 April 2025
Accepted: 25 April 2025
Published: 27 April 2025

Citation: Agnihotri, A.; Kumar, V.; Suhonen, J. Correlating the $0\nu\beta\beta$-Decay Amplitudes of ^{136}Xe with the Ordinary Muon Capture (OMC) Rates of ^{136}Ba. *Universe* **2025**, *11*, 138. https://doi.org/10.3390/universe11050138

1. Introduction

The theoretical study of the hypothesized rare neutrinoless double beta ($0\nu\beta\beta$) decay is challenging, yet it is among the most promising avenues of physics research beyond the standard model [1–5]. The complexity in the study of $0\nu\beta\beta$ decay stems from the involvement of nuclear-structure effects/correlations from low to high momentum-exchange scales ($q \leq 100 - 200$ MeV) and nuclear states of high energy and/or multipolarity (J^π). Experimental nuclear-structure data at medium and high momentum scales are seldom available and are almost entirely uncharted territory, making it difficult for nuclear models and, hence, the computed $0\nu\beta\beta$ nuclear matrix elements (NMEs) to be improved upon being tuned to such data. Given that $0\nu\beta\beta$ decay has not been measured, accurate nuclear modeling of this process for various $0\nu\beta\beta$-decay candidates is essential for determining the sensitivity of experiments designed to detect this rare decay [6]. There are significant discrepancies in the $0\nu\beta\beta$-decay NMEs computed in various nuclear-model frameworks [1], and imperfect nuclear-structure calculations demand the use of an effective value of the axial vector coupling (g_A^{eff}) [5–8]. Discrepancies in $0\nu\beta\beta$-decay NMEs across nuclear models and uncertainty in the value of g_A^{eff} propagate in the 2nd and 4th powers, respectively, to the computed/predicted half-lives.

Ordinary muon capture (OMC) is a seemingly miraculous process in that it is the only known practical way to systematically investigate the nuclear structure experimentally at momentum scales relevant to the physics of $0\nu\beta\beta$ decay [9–12]. OMC can also populate all

the nuclear states that are intermediate states of the odd–odd nucleus, via which the $0\nu\beta\beta$ decay proceeds [9–12]. This means that OMC can and is used to access decay amplitudes of one leg, involving either the daughter or the mother nucleus of the "two-step" rare transition, depending on whether $0\nu\beta\beta$ is of β^- or β^+/EC type, respectively [9–13]. Involvement of common decay amplitudes in this way for the computed OMC NMEs/rates and $0\nu\beta\beta$-decay NMEs leads us to look for connections between the two. Towards both ends of computing more accurate $0\nu\beta\beta$-decay NMEs and determination of g_A^{eff}, the OMC process is a gift from nature as it can help address both of these goals. The study of OMC is the best-known way to test the fitness of nuclear models and improve their accuracy, by closely tuning them to experimental data for computing physically relevant OMC NMEs. Tuning the nuclear models this way makes them optimized to compute $0\nu\beta\beta$-decay amplitudes and ultimately NMEs due to similar nuclear and weak-interaction contributions involved in the two processes [10–12,14]. As an example, OMC can give us access to the value of the particle–particle interaction parameter (g_{pp}) in the pnQRPA (proton–neutron quasiparticle random-phase approximation) framework [10–12], and g_A^{eff} and/or the effective value of the pseudoscalar coupling (g_P) [15–29] at momentum scales relevant for $0\nu\beta\beta$ decay. Recent calculations of OMC rates were performed in [30].

Only in the recent past have major experimental efforts been made to leverage OMC to illuminate further the mystery of $0\nu\beta\beta$ decay, by measuring (partial) OMC rates, as performed in present state-of-the-art experiments such as the MONUMENT experiment [31]. Such experiments will make available invaluable experimental constraints for grounding the theoretical modeling of OMC processes, offering a tangible map for the improvement of nuclear models, and leading the way to more accurate computed OMC/$0\nu\beta\beta$-decay NMEs.

The connection of having common decay amplitudes in the computed NMEs of the two processes prompted the search for the potential correlations and trends between $0\nu\beta\beta$-decay NMEs and OMC rates/NMEs, as presented in References [10–12,32]. Such connections can be used to determine the accuracy of the computed $0\nu\beta\beta$-decay NMEs. In Reference [32], average OMC NMEs and $0\nu\beta\beta$-decay NMEs for key $0\nu\beta\beta$-decay candidates including ^{136}Xe (the focus of this work), were compared in the framework of pnQRPA, and systematic correspondences were observed between the two. The NMEs were compared in order to minimize the kinematic and phase-space effects in the anticipated correlations. Given the trends observed in Reference [32], we anticipate seeing this correspondence map to correspondences between OMC rates and $0\nu\beta\beta$-decay NMEs. Evidence for such a connection is foreshadowed from trends between OMC rates and $2\nu\beta\beta$-decay NMEs, as presented in References [10–12]. Correlations between OMC rates and $0\nu\beta\beta$-decay NMEs are of high interest, as this can be a direct bridge between experimental OMC rates and theoretical $0\nu\beta\beta$-decay NMEs.

The focus of this work is to further elucidate this bridge in the context of $0\nu\beta\beta$ decaying ^{136}Xe, using, for the first time, the pnQRPA and nuclear shell model (NSM) together in OMC and non-closure $0\nu\beta\beta$ formalisms. We compute the $0\nu\beta\beta$-decay amplitudes in the above frameworks and compare them with results obtained for the OMC rates of ^{136}Ba, as presented in Reference [33], using the same nuclear models. In using different nuclear models, one can see if the potential correlations are model-independent and follow the similarities and differences in the trends that emerge.

2. Theory

2.1. Nuclear-Model Calculations

In the present work, we adopt the nuclear shell model (NSM) and the proton–neutron quasiparticle random-phase approximation (pnQRPA) [34] as the basic nuclear-model

frameworks. We compute the wave functions of the states of the odd–odd nucleus ^{136}Cs by using these models in order to access the $0\nu\beta\beta$-decay amplitudes in a non-closure approach and compare them with the corresponding OMC rates computed in Reference [33]. In both the OMC and $0\nu\beta\beta$ calculations we use the phenomenological NSM (**sm-phen**) and pnQRPA (**qrpa-phen**) approach, with the relevant parameters defined in Table 1 of Reference [33]. As in [33], the decay amplitudes are computed for states with excitation energy ≤ 1 MeV, an energy range relevant to present-day MONUMENT experiment [31].

In order to give the reader a brief glimpse of the parameters used in the calculations, we repeat here some of the information given in full length in Ref. [33]. For the NSM calculations, we chose the jj55pn model space with the 2s-1d-0$g_{7/2}$-0$h_{11/2}$ set of single-particle orbitals for both protons and neutrons. We use the sn100pn interaction [35] and we use the quenching factor $q = 0.74$ benchmarked by the works [36–38], leading to the effective axial coupling of $g_A^{eff} = 0.93$. We determine the value of the pseudoscalar coupling g_P by using the Godberger–Treiman partially conserved axial vector current (PCAC) hypothesis $g_P/g_A \approx 6.8$. For more details, see [33].

For the pnQRPA, we use the no-core valence space of Ref. [39] based on the Woods–Saxon parameters of Ref. [40] modified slightly at the proton and neutron Fermi surfaces in order to better reproduce the single-quasiparticle type of spectra of the neighboring odd-A nuclei. We use the Bonn-A G-matrix interaction [41] with the BCS (Bardeen–Cooper–Schriefer) mean field defined by the pairing-parameter values $g_p^{pair} = 0.83$ for protons and $g_n^{pair} = 0.87$ for neutrons, fitted to reproduce the available phenomenological proton and neutron separation energies in ^{136}Ba [34]. The beyond-BCS mean field effective residual interaction is defined using the particle-hole parameter $g_{ph} = 1.18$, fitted to the experimental energy of the Gamow–Teller giant resonance. For the particle–particle channel, we use the renormalization scheme introduced in [42] by dividing the corresponding strength parameter to the isoscalar $g_{pp}^{T=0} = 0.7$ and isovector $g_{pp}^{T=1} = 0.7$ parts, the values taken from Ref. [39]. For the weak axial coupling, we use the value $g_A^{eff} = 0.83$ taken from the systematics obtained in [43]. For the weak pseudoscalar coupling, we use the recipe adopted for the NSM above.

An interesting additional point could be raised here: Our adopted pnQRPA framework is based on a spherical single-particle mean field. This should be contrasted with the fact that the nucleus ^{136}Xe is spherical but the nucleus ^{136}Ba shows signs of deformation, as seen, e.g., in its excitation spectrum. This mismatch of shapes of the $0\nu\beta\beta$ mother and daughter nuclei is a well-known driver of the suppression of the magnitude $0\nu\beta\beta$ NME through the pnQRPA overlap factor present in Equation (8) below [44–46]. This feature naturally affects the accuracy of both the OMC rate calculations and the right-leg virtual amplitudes of the $0\nu\beta\beta$ decay. However, as both the OMC and $0\nu\beta\beta$ calculations are affected by the same inaccuracy, the correlations found between the two processes are most likely not altered much. A similar argument supports the view that also the correlations found in the NSM calculations are robust and are not affected by the difference in deformations of the two nuclei.

2.2. Ordinary Muon Capture (OMC)

The OMC is a well-studied nuclear process, both experimentally and theoretically [9]. In this work, we compare our calculated $0\nu\beta\beta$-decay amplitudes with the OMC rates of Reference [33]. The OMC formalism of Reference [33] is an extended Morita–Fujii formalism described in detail in [47,48]. Lately, the use of realistic muon wave functions has been implemented [49], and up-to-date computations for OMC rates of ^{136}Ba are presented in Reference [33]. We refer readers to these results, as we use them for the purposes of this

work. For completeness, we present here some key relations for computing the OMC rates, where OMC of ^{136}Ba proceeds as follows:

$$\mu^- + ^{136}\mathrm{Ba}(0^+_{g.s.}) \rightarrow \nu_\mu + ^{136}\mathrm{Cs}(J^\pi_f), \tag{1}$$

where a negative muon (μ^-) is captured by the atomic 1s ground state of ^{136}Ba, leading to final spin-parity states J^π_f in ^{136}Cs. At the same time, a muon neutrino (ν_μ) is emitted. The general expression of the OMC rate is given as follows:

$$W = 2P(2J_f + 1)\left(1 - \frac{q}{m_\mu + AM}\right)q^2, \tag{2}$$

where the momentum exchange q is expressed as

$$q = (m_\mu - W_0)\left(1 - \frac{m_\mu}{2(m_\mu + AM)}\right). \tag{3}$$

Here, J_f is the final-state spin-parity, M is the average nucleon mass, A is the nuclear mass number, and m_μ (m_e) is the rest mass of the muon (electron). The threshold energy is given by

$$W_0 = M_f - M_i + m_e + E_X, \tag{4}$$

where M_i and M_f are the masses of the initial and final nuclei, and E_X is the excitation energy of the final nuclear state, in our case of ^{136}Cs. The rate function P contains the NMEs, phase-space factors, and combinations of weak couplings g_A (axial-vector), g_P (induced pseudoscalar), and $g_M = 1 + \mu_p - \mu_n$ (induced weak-magnetism), with μ_p and μ_n being the anomalous magnetic moments of the proton and neutron, respectively.

2.3. $0\nu\beta\beta$ Decay

The computational scheme used here is presented in detail in Reference [50]. We present here key relations. Assuming light Majorana neutrino exchange [4,50], the inverse half-life can be written as

$$\left[t^{(0\nu)}_{1/2}(0^+_i \rightarrow 0^+_f)\right]^{-1} = g^4_A G_{0\nu}\left|M^{(0\nu)}\right|^2 |\langle m_\nu\rangle|^2, \tag{5}$$

where $G_{0\nu}$ is the phase-space factor for the final-state leptons, g_A is the axial vector coupling constant, $\langle m_\nu\rangle$ is the effective neutrino mass, and $M^{(0\nu)}$ is the nuclear matrix element (NME). The $M^{(0\nu)}$ NME can be decomposed as follows:

$$M^{(0\nu)} = M^{(0\nu)}_{\mathrm{GT}} - \left(\frac{g_V}{g_A}\right)^2 M^{(0\nu)}_{\mathrm{F}} + M^{(0\nu)}_{\mathrm{T}}, \tag{6}$$

where $M^{(0\nu)}_{\mathrm{GT}}$, $M^{(0\nu)}_{\mathrm{F}}$, and $M^{(0\nu)}_{\mathrm{T}}$ are the Gamow–Teller, Fermi, and Tensor components of the NME, respectively, and g_V is the vector coupling constant. Contribution from various multipoles constituting all the intermediate transitions is given as follows:

$$M^{(0\nu)}_K = \sum_{J^\pi} M^{(0\nu)}_K(J^\pi), \tag{7}$$

where $K = \mathrm{GT}, \mathrm{F}, \mathrm{T}$, and $M^{(0\nu)}_K(J^\pi)$ are the contributions from all the states i of the intermediate multipole J^π. Each multipole contribution is, in turn, decomposed in terms of the

two-particle transition matrix elements and one-body transition densities. In the pnQRPA calculations, the two-particle transition matrix element reads

$$M_K^{(0\nu)}(J^\pi) = \sum_{k_1,k_2,J'} \sum_{pp',nn'} (-1)^{j_n+j_{p'}+J+J'} \sqrt{2J'+1} \begin{Bmatrix} j_p & j_n & J \\ j_{n'} & j_{p'} & J' \end{Bmatrix} \times \\ (pp' : J'|O_K|nn' : J') \left(0_f^+ |||[c_{p'}^\dagger \tilde{c}_n]_J||| J_{k_1}^\pi\right) \langle J_{k_1}^\pi | J_{k_2}^\pi \rangle \left(J_{k_2}^\pi |||[c_p^\dagger \tilde{c}_n]_J||| 0_i^+\right), \quad (8)$$

where k_1, k_2 label the pnQRPA solutions for a given multipole J^π, starting from the final (k_1) and initial (k_2) nuclei, and p, p', n, n' denote the proton and neutron single-particle quantum numbers. The operator O_K contains the neutrino potentials, the characteristic two-particle operators for the different K components, and short-range correlation effects. The quantities $\left(0_f^+ |||[c_{p'}^\dagger \tilde{c}_n]_J||| J_{k_1}^\pi\right)$ and $\left(J_{k_2}^\pi |||[c_p^\dagger \tilde{c}_n]_J||| 0_i^+\right)$ are the corresponding decay amplitudes, and $\langle J_{k_1}^\pi | J_{k_2}^\pi \rangle$ is an overlap factor connecting the two branches of pnQRPA solutions for the ^{136}Cs wave functions.

In the NSM calculations, we use one unique set of states in ^{136}Cs so that the sum over k_1, k_2 in Equation (8) is replaced by a sum over a single state number k and the overlap factor is not needed.

3. Results and Discussion

In order to compare the OMC rates and $0\nu\beta\beta$-decay amplitudes for J_k^π states in a meaningful way, we consider the following physical assumptions: both quantities depend on the energy ($E_k(J_k^\pi)$), multipolarity (J^π), and nuclear-structure content of the J_k^π (virtual) states being populated in the process. In the case of OMC rates, phase-space factors contribute directly to OMC rates. For $0\nu\beta\beta$-decay NMEs, the dependence of neutrino potentials on energy affects the concerned decay amplitudes. For our analysis, we can assume the energy dependence to be a constant for all the states as their energy is $\leq$1 MeV. Therefore, our analysis simplifies, and we attribute the observed trends in OMC rates and $0\nu\beta\beta$-decay amplitudes to multipolarity (J^π) and nuclear-structure content of J_k^π states. We see effects of such dependencies in the computed $0\nu\beta\beta$-decay amplitudes presented in Tables 1 and 2 for the aforementioned computational scheme in Section 2.1.

Table 1. Phenomenological pnQRPA-computed $0\nu\beta\beta$-decay amplitudes of the NMEs of Equation (6). The amplitudes are given in units of 10^{-3}.

J^π	E_{exc} [keV]	M_{F}	M_{GT}	M_{T}	$M^{(0\nu)}$
5_1^+	0	0	−0.18	0.040	−0.14
3_1^+	102	0	−0.28	0.037	−0.24
2_1^+	120	0.20	−0.13	−0.034	−0.46
4_1^+	154	0.07	−0.02	−0.006	−0.13
1_1^+	193	0	−1.61	0.021	−1.59
4_2^+	203	4.96	−0.32	−0.13	−7.65
3_2^+	264	0	−51.6	16.3	−35.2
3_3^+	281	0	−10.1	0.88	−9.20
3_4^+	338	0	−9.46	−3.27	−12.7
2_2^+	367	0.01	−0.16	−0.0041	−0.22
3_1^-	458	0.02	−0.16	−0.0060	−0.25
4_3^+	494	−0.007	−0.24	−0.089	−0.32
5_1^-	515	0.03	−0.11	−0.050	−0.21
4_1^-	558	0	−0.42	0.068	−0.35
2_3^+	561	5.29	−24.5	−8.22	−40.4
5_2^-	637	0.07	−0.01	−0.004	−0.12
4_2^-	695	0	−0.24	0.084	−0.16
2_1^-	704	0	−0.49	0.097	−0.40
3_2^-	926	0.23	−0.02	−0.008	−0.36

Table 2. Phenomenological NSM-computed $0\nu\beta\beta$-decay amplitudes of the NMEs of Equation (6). The amplitudes are given in units of 10^{-3}.

J^π	$E_{\rm exc}$ [keV]	$M_{\rm F}$	$M_{\rm GT}$	$M_{\rm T}$	$M^{(0\nu)}$
5^+_1	0	0	−4.355	1.411	−2.944
3^+_1	23	0	−5.695	1.445	−4.250
4^+_1	39	1.230	−0.153	−0.058	−1.633
2^+_1	83	6.993	−5.160	−1.433	−14.677
3^+_2	181	0	−2.269	−0.555	−2.824
2^+_2	224	0.894	−4.481	−1.748	−7.262
3^+_3	244	0	−1.647	−0.059	−1.706
4^+_2	323	1.989	−2.575	−1.019	−5.895
4^+_3	498	2.582	−3.525	−1.578	−8.088
3^+_4	517	0	6.540	−0.289	6.251
5^-_1	522	0.723	−2.483	−1.048	−4.366
3^-_1	545	0.379	−4.893	−1.701	−7.033
1^+_1	545	0	33.820	−1.602	32.218
4^-_1	547	0	5.565	0.589	6.154
2^+_3	615	−1.426	2.804	0.780	5.232
5^-_2	670	1.313	−0.511	−0.210	−2.239
1^+_2	752	0	6.066	−0.064	6.003
4^-_2	760	0	−1.281	0.309	−0.972
2^+_4	803	0.290	−0.889	−0.251	−1.475
4^+_4	885	0.082	−0.108	−0.044	−0.248
2^-_1	1016	0	−44.144	0.371	−43.772

Computed OMC rates for individual J^π_k states can be found in Reference [33]. In order to smooth out the variations of the OMC rates and $0\nu\beta\beta$-decay amplitudes from one individual J^π state to the other, we study the combined contribution to a given multipole J^π, an effective strategy already implemented in Reference [32]. Another important consideration is that, given that the nuclear-structure calculations are not perfect, we only consider the trends within the same nuclear model. Therefore, for the purposes of this paper, we look at trends in pnQRPA (**qrpa-phen**) and NSM (**sm-phen**) results independently. In Table 3, the cumulative OMC rates OMC(J^π) and amplitude contributions to $M^{(0\nu)}(J^\pi)$ for multipole J^π are given, and are also plotted in Figures 1 and 2.

Table 3. Cumulative $0\nu\beta\beta$-decay amplitudes $M^{(0\nu)}(J^\pi)$ and OMC rates OMC(J^π) for multipoles $J^\pi \leq 5$. OMC rates and the decay amplitudes are given in units of 10^3 1/s and 10^{-3}, respectively.

	qrpa-phen		**sm-phen**	
J^π	$M^{(0\nu)}(J^\pi)$	OMC(J^π)	$M^{(0\nu)}(J^\pi)$	OMC(J^π)
5^+	−0.14	0.50	−2.944	0.0
4^+	−8.10	20.4	−15.864	9.8
3^+	−57.4	87.8	−2.529	29.9
2^+	−41.0	201.1	−18.182	34.9
1^+	−1.59	206.9	38.221	5.2
5^-	−0.33	0.80	−6.605	0.6
4^-	−0.52	21.2	5.182	15.0
3^-	−0.61	38.7	−7.033	9.7
2^-	−0.40	14.2	−43.772	44.4

In the figures, positive and negative multipoles are plotted separately for clarity, and the quantities are scaled appropriately for optimal comparison. As seen from the plots in Figures 1 and 2, regular variations between the quantities are observed. The variation of OMC rates (J^π) and $M^{(0\nu)}(J^\pi)$ appear to be roughly "mirror reflections" of each other, both in the context of pnQRPA and NSM. Further conclusions cannot be made given the limited number of states and multipolarity, but the results look promising, giving impetus to a larger-scale study involving a larger set of states for each multipolarity, and covering a larger range of multipolarities, possibly for the Gamow–Teller giant resonance region in the case of the pnQRPA.

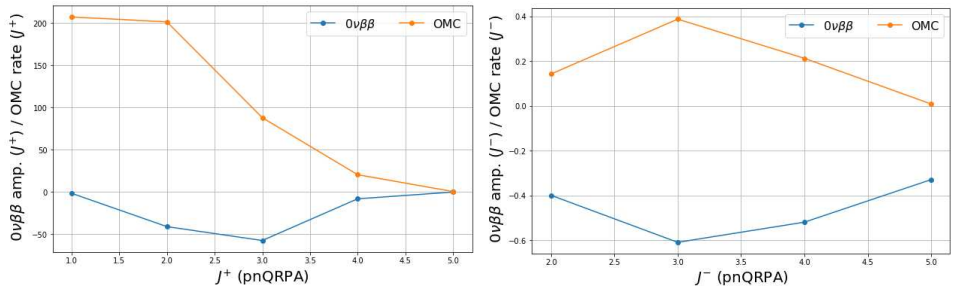

(**a**) (**b**)

Figure 1. Cumulative $0\nu\beta\beta$-decay amplitudes and OMC rates for J^π states computed using pnQRPA (**qrpa-phen**). The decay amplitudes and OMC rates are scaled appropriately for optimal comparison. (**a**) $M^{(0\nu)}(J^+)$ (in units of 10^{-3}) and OMC(J^+) (in units of 10^3 1/s) vs. J^+; (**b**) $M^{(0\nu)}(J^-)$ (in units of 10^{-3}) and OMC(J^-) (in units of 10^5 1/s) vs. J^-.

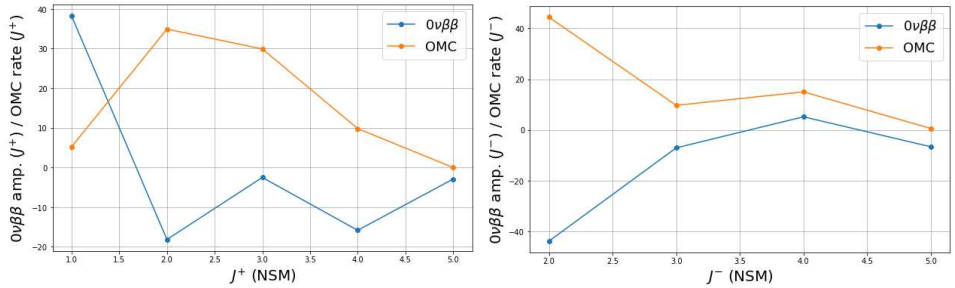

(**a**) (**b**)

Figure 2. Cumulative $0\nu\beta\beta$-decay amplitudes and OMC rates for J^π states computed using NSM (**sm-phen**). The decay amplitudes and OMC rates have been scaled appropriately for optimal comparison. (**a**) $M^{(0\nu)}(J^+)$ (in units of 10^{-3}) and OMC(J^+) (in units of 10^3 1/s) vs. J^+; (**b**) $M^{(0\nu)}(J^-)$ (in units of 10^{-3}) and OMC(J^-) (in units of 10^3 1/s) vs. J^-.

In order to shed further light on the comparison of the OMC and $0\nu\beta\beta$ results, one can plot the absolute values of $0\nu\beta\beta$ amplitudes $|M^{(0\nu)}|$ ($0\nu\beta\beta$ NME for short) against the absolute values of the average OMC nuclear matrix elements $|M^\mu|_{\rm ave}$ (OMC NME for short), defined in [32] as

$$W = 2\pi |M^\mu|^2_{\rm ave} q^2 \frac{dq}{dE_f}, \tag{9}$$

with the detailed expression of $|M^\mu|_{\rm ave}$ given in [32]. As performed in [32], we can plot the cumulative percentages of $|M^{(0\nu)}|$ and $|M^\mu|_{\rm ave}$ as functions of the excitation energy of the individual J^π states below 1 MeV of excitation in ^{136}Cs. This is shown in Figure 3.

As can be seen in Figure 3, both for the NSM and the pnQRPA, the two absolute NMEs follow each other's trends rather closely. This is particularly true for the NSM, where the big jump in the cumulative absolute values happens at the same energy for both models. For the pnQRPA, two almost vertical jumps are visible for the $0\nu\beta\beta$ NME, whereas for the OMC NME, the corresponding jumps are softer but are still located in the same energy regions as those of the $0\nu\beta\beta$ NME. This comparison could be extended to higher intermediate energies once data on OMC rates become available. Through the potential data, one can access the OMC NME $|M^\mu|_{\rm ave}$ as a function of the excitation energy and, in principle, correct $|M^{(0\nu)}|$ accordingly at large jumps of the OMC NME.

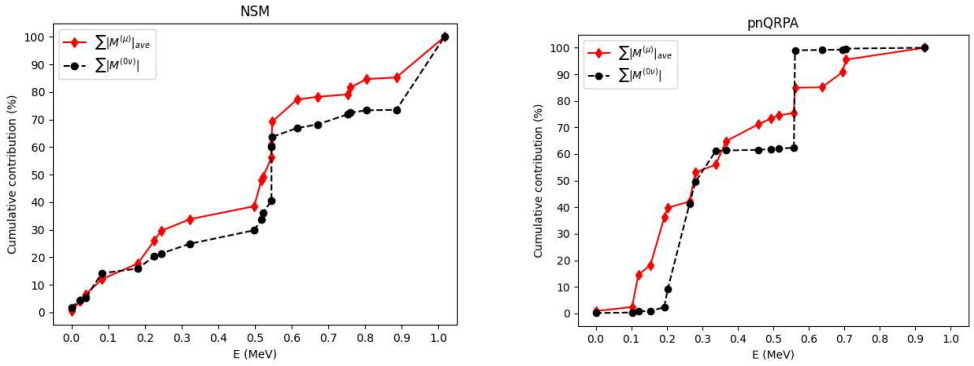

(**a**) (**b**)

Figure 3. Comparison of the cumulative percentage contributions to the matrix elements $|M^{(0\nu)}|$ and $|M^{\mu}|_{\rm ave}$ as functions of the excitation energy in ^{136}Cs. (**a**) Cumulative contributions for NSM. (**b**) Cumulative contribution for pnQRPA.

4. Conclusions

Correlations between the ordinary muon capture (OMC) on ^{136}Ba and $0\nu\beta\beta$ decay of ^{136}Xe were searched for using $0\nu\beta\beta$-decay intermediate states in ^{136}Cs below 1 MeV of excitation and for angular-momentum values $J \leq 5$. We computed $0\nu\beta\beta$-decay amplitudes through these intermediate states by using the proton–neutron quasiparticle random-phase approximation (pnQRPA) and nuclear shell model (NSM). Comparison with a corresponding earlier OMC calculation suggests that there are "mirror type of" correlations between the $0\nu\beta\beta$-decay amplitudes and the OMC rates, in addition to rather strong correlations in the cumulative values of the OMC and $0\nu\beta\beta$ "nuclear matrix elements". These correlations suggest that an extension of the present analysis to a wider energy and angular-momentum region could lead to a practical way to probe the $0\nu\beta\beta$-decay nuclear matrix elements using experimental data on OMC rates to intermediate states of $0\nu\beta\beta$ decays.

Author Contributions: Calculation of $0\nu\beta\beta$-decay amplitudes using NSM, figures, primary analyses, writing the first draft: A.A.; NSM calculations, preparation of $0\nu\beta\beta$ calculation input files for NSM (used by A.A.), figures: V.K.; original idea of the project, computing $0\nu\beta\beta$-decay amplitudes using pnQRPA, coordination and supervision of the computations and analyses, analyses, finalizing the text of the draft: J.S. All authors have read and agreed to the published version of the manuscript.

Funding: A.A. and J.S. acknowledge support from project PNRR-I8/C9-CF264, Contract No. 760100/23.5.2023 of the Romanian Ministry of Research, Innovation and Digitization (the NEPTUN project). V.K. acknowledges financial support from "GEFP" IoE BHU fellowship (R/Dev/D/IoE/2024-25/GEFP/76559), and SERB Project (File No. EEQ/2023/000157), Govt. of India.

Data Availability Statement: Data are contained within the article.

Acknowledgments: We acknowledge grants of computer capacity from the Finnish Grid and Cloud Infrastructure (persistent identifier urn:nbn:fi:research-infras-2016072533), the support by CSC–IT Center for Science, Finland, for the generous computational resources.

Conflicts of Interest: The authors declare no conflicts of interest.

References

1. Agostini, M.; Benato, G.; Detwiler, J.A.; Menéndez, J.; Vissani, F. Toward the discovery of matter creation with neutrinoless $\beta\beta$ decay. *Rev. Mod. Phys.* **2023**, *95*, 025002. [CrossRef]
2. Blaum, K.; Eliseev, S.; Danevich, F.A.; Tretyak, V.I.; Kovalenko, S.; Krivoruchenko, M.I.; Novikov, Y.N.; Suhonen, J. Neutrinoless double-electron capture. *Rev. Mod. Phys.* **2020**, *92*, 045007. [CrossRef]

3. Engel, J.; Menéndez, J. Status and future of nuclear matrix elements for neutrinoless double-beta decay: A review. *Rep. Prog. Phys.* **2017**, *80*, 046301. [CrossRef] [PubMed]
4. Suhonen, J.; Civitarese, O. Weak-interaction and nuclear-structure aspects of nuclear double beta decay. *Phys. Rep.* **1998**, *300*, 123–214. [CrossRef]
5. Ejiri, H.; Suhonen, J.; Zuber, K. Neutrino–nuclear responses for astro-neutrinos, single beta decays and double beta decays. *Phys. Rep.* **2019**, *797*, 1. [CrossRef]
6. Suhonen, J. Impact of the quenching of g_{A} on the sensitivity of $0\nu\beta\beta$ experiments. *Phys. Rev. C* **2017**, *96*, 055501. [CrossRef]
7. Suhonen, J.T. Value of the Axial-Vector Coupling Strength in β and $\beta\beta$ Decays: A Review. *Front. Phys.* **2017**, *5*, 55. [CrossRef]
8. Suhonen, J.; Kostensalo, J. Double β Decay and the Axial Strength. *Front. Phys.* **2019**, *7*, 29. [CrossRef]
9. Measday, D. The nuclear physics of muon capture. *Phys. Rep.* **2001**, *354*, 243–409. [CrossRef]
10. Kortelainen, M.; Suhonen, J. Ordinary muon capture as a probe of virtual transitions of $\beta\beta$ decay. *Europhys. Lett.* **2002**, *58*, 666. [CrossRef]
11. Kortelainen, M.; Suhonen, J. Microscopic study of muon-capture transitions in nuclei involved in double-beta-decay processes. *Nucl. Phys. A* **2003**, *713*, 501–521. [CrossRef]
12. Kortelainen, M.; Suhonen, J. Nuclear muon capture as a powerful probe of double-beta decays in light nuclei. *J. Phys. Nucl. Part. Phys.* **2004**, *30*, 2003. [CrossRef]
13. Jokiniemi, L.; Suhonen, J.; Kotila, J. Comparative analysis of nuclear matrix elements of $0\nu\beta^+\beta^+$ decay and muon capture in ^{106}Cd. *Front. Phys.* **2021**, *9*, 652536. [CrossRef]
14. Šimkovic, F.; Pantis, G.; Vergados, J.D.; Faessler, A. Additional nucleon current contributions to neutrinoless double β decay. *Phys. Rev. C* **1999**, *60*, 055502. [CrossRef]
15. Kolbe, E.; Langanke, K.; Vogel, P. Muon capture, continuum random phase approximation, and in-medium renormalization of the axial-vector coupling constant. *Phys. Rev. C* **1994**, *50*, 2576–2581. [CrossRef] [PubMed]
16. Johnson, B.L.; Gorringe, T.P.; Armstrong, D.S.; Bauer, J.; Hasinoff, M.D.; Kovash, M.A.; Measday, D.F.; Moftah, B.A.; Porter, R.; Wright, D.H. Observables in muon capture on ^{23}Na and the effective weak couplings $\tilde{g_a}$ and $\tilde{g_p}$. *Phys. Rev. C* **1996**, *54*, 2714–2731. [CrossRef]
17. Gorringe, T.P.; Armstrong, D.S.; Arole, S.; Boleman, M.; Gete, E.; Kuzmin, V.; Moftah, B.A.; Sedlar, R.; Stocki, T.J.; Tetereva, T. Measurement of partial muon capture rates in $1s-0d$ shell nuclei. *Phys. Rev. C* **1999**, *60*, 055501. [CrossRef]
18. Siiskonen, T.; Suhonen, J.; Hjorth-Jensen, M. Shell-model effective operators for muon capture in ^{20}Ne. *J. Phys. Nucl. Part. Phys.* **1999**, *25*, L55. [CrossRef]
19. Siiskonen, T.; Hjorth-Jensen, M.; Suhonen, J. Renormalization of the weak hadronic current in the nuclear medium. *Phys. Rev. C* **2001**, *63*, 055501. [CrossRef]
20. Auerbach, N.; Brown, B.A. Weak interaction rates involving ^{12}C, ^{14}N, and ^{16}O. *Phys. Rev. C* **2002**, *65*, 024322. [CrossRef]
21. Gorringe, T.P.; Johnson, B.L.; Armstrong, D.S.; Bauer, J.; Kovash, M.A.; Hasinoff, M.D.; Measday, D.F.; Moftah, B.A.; Porter, R.; Wright, D.H. Hyperfine effect in μ^- capture on ^{23}Na and g_p/g_a. *Phys. Rev. Lett.* **1994**, *72*, 3472–3475. [CrossRef] [PubMed]
22. Jonkmans, G.; Ahmad, S.; Armstrong, D.S.; Azuelos, G.; Bertl, W.; Blecher, M.; Chen, C.Q.; Depommier, P.; Doyle, B.C.; von Egidy, T.; et al. Radiative Muon Capture on Hydrogen and the Induced Pseudoscalar Coupling. *Phys. Rev. Lett.* **1996**, *77*, 4512–4515. [CrossRef]
23. Gazit, D. Muon capture on ^{3}He and the weak structure of the nucleon. *Phys. Lett. B* **2008**, *666*, 472–476. [CrossRef]
24. Marcucci, L.E.; Kievsky, A.; Rosati, S.; Schiavilla, R.; Viviani, M. Chiral Effective Field Theory Predictions for Muon Capture on Deuteron and ^{3}He. *Phys. Rev. Lett.* **2012**, *108*, 052502. [CrossRef]
25. Brudanin, V.; Egorov, V.; Filipova, T.; Kachalkin, A.; Kovalenko, V.; Salamatin, A.; Shitov, Y.; Štekl, I.; Vassiliev, S.; Vorobel, V.; et al. Measurement of the induced pseudoscalar form factor in the capture of polarized muons by Si nuclei. *Nucl. Phys. A* **1995**, *587*, 577–595. [CrossRef]
26. Siiskonen, T.; Suhonen, J.; Kuz'min, V.; Tetereva, T. Shell-model study of partial muon-capture rates in light nuclei. *Nucl. Phys. A* **1998**, *635*, 446–469. [CrossRef]
27. Siiskonen, T.; Suhonen, J.; Kuz'min, V.; Tetereva, T. Shell-model study of partial muon-capture rates in light nuclei. *Nucl. Phys. A* **1999**, *651*, 437–438. [CrossRef]
28. Siiskonen, T.; Suhonen, J.; Hjorth-Jensen, M. Towards the solution of the C_P/C_A anomaly in shell-model calculations of muon capture. *Phys. Rev. C* **1999**, *59*, R1839–R1843. [CrossRef]
29. Gorringe, T.; Fearing, H.W. Induced pseudoscalar coupling of the proton weak interaction. *Rev. Mod. Phys.* **2003**, *76*, 31–91. [CrossRef]
30. Šimkovic, F.; Dvornický, R.; Vogel, P. Muon capture rates: Evaluation within the quasiparticle random-phase approximation. *Phys. Rev. C* **2020**, *102*, 034301. [CrossRef]
31. Araujo, G.R.; Bajpai, B.D.; Baudis, L.; Belov, V.; Bossio, E.; Cocolios, T.E.; Ejiri, H.; Fomina, F.; Gusev, K.; Hashim, I.H.; et al. The MONUMENT experiment: Ordinary muon capture studies for $0\nu\beta\beta$ decay. *Eur. Phys. J. C* **2024**, *84*, 1188. [CrossRef]

32. Jokiniemi, L.; Suhonen, J. Comparative analysis of muon-capture and $0\nu\beta\beta$-decay matrix elements. *Phys. Rev. C* **2020**, *102*, 024303. [CrossRef]
33. Gimeno, P.; Jokiniemi, L.; Kotila, J.; Ramalho, M.; Suhonen, J. Ordinary Muon Capture on ^{136}Ba: Comparative Study Using the Shell Model and pnQRPA. *Universe* **2023**, *9*, 270. [CrossRef]
34. Suhonen, J. *From Nucleons to Nucleus: Concepts of Microscopic Nuclear Theory*; Springer: Berlin/Heidelberg, Germany, 2007.
35. Brown, B.A.; Stone, N.J.; Stone, J.R.; Towner, I.S.; Hjorth-Jensen, M. Magnetic moments of the 2_1^+ states around ^{132}Sn. *Phys. Rev. C* **2005**, *71*, 044317. [CrossRef]
36. Caurier, E.; Nowacki, F.; Poves, A.; Retamosa, J. Shell Model Studies of the Double Beta Decays of ^{76}Ge, ^{82}Se, and ^{136}Xe. *Phys. Rev. Lett.* **1996**, *77*, 1954–1957. [CrossRef] [PubMed]
37. Caurier, E.; Menéndez, J.; Nowacki, F.; Poves, A. Influence of Pairing on the Nuclear Matrix Elements of the Neutrinoless $\beta\beta$ Decays. *Phys. Rev. Lett.* **2008**, *100*, 052503. [CrossRef] [PubMed]
38. Horoi, M.; Brown, B.A. Shell-Model Analysis of the ^{136}Xe Double Beta Decay Nuclear Matrix Elements. *Phys. Rev. Lett.* **2013**, *110*, 222502. [CrossRef]
39. Jokiniemi, L.; Ejiri, H.; Frekers, D.; Suhonen, J. Neutrinoless $\beta\beta$ nuclear matrix elements using isovector spin-dipole $J^\pi = 2^-$ data. *Phys. Rev. C* **2018**, *98*, 024608. [CrossRef]
40. Bohr, A.; Mottelson, B.R. *Nuclear Structure*; Benjamin: New York, NY, USA, 1969; Volume I.
41. Holinde, K. Two-nucleon forces and nuclear matter. *Phys. Rep.* **1981**, *68*, 121–188. [CrossRef]
42. Šimkovic, F.; Rodin, V.; Faessler, A.; Vogel, P. $0\nu\beta\beta$ and $2\nu\beta\beta$ nuclear matrix elements, quasiparticle random-phase approximation, and isospin symmetry restoration. *Phys. Rev. C* **2013**, *87*, 045501. [CrossRef]
43. Pirinen, P.; Suhonen, J. Systematic approach to β and $2\nu\beta\beta$ decays of mass $A = 100 - 136$ nuclei. *Phys. Rev. C* **2015**, *91*, 054309. [CrossRef]
44. Yusef, M.; Rodin, V.; Faessler, A.; Šimkovic, F. Two-neutrino double β decay of deformed nuclei within the quasiparticle random-phase approximation with a realistic interaction. *Phys. Rev. C* **2009**, *79*, 014314. [CrossRef]
45. Fang, D.; Faessler, A.; Rodin, V. Neutrinoless double-β decay of deformed nuclei within quasiparticle random-phase approximation with a realistic interaction. *Phys. Rev. C* **2011**, *83*, 034320. [CrossRef]
46. Fang, D.; Faessler, A.; Šimkovic, F. $0\nu\beta\beta$-decay nuclear matrix element for light and heavy neutrino mass mexhanisms from deformed quasiparticle random-phase approximation calculations for ^{76}Ge, ^{82}Se, ^{130}Te, ^{136}Xe, and ^{150}Nb with isospin restoration. *Phys. Rev. C* **2018**, *97*, 045503. [CrossRef]
47. Jokiniemi, L.; Suhonen, J.; Ejiri, H.; Hashim, I. Pinning down the strength function for ordinary muon capture on ^{100}Mo. *Phys. Lett. B* **2019**, *794*, 143–147. [CrossRef]
48. Jokiniemi, L.; Suhonen, J. Muon-capture strength functions in intermediate nuclei of $0\nu\beta\beta$ decays. *Phys. Rev. C* **2019**, *100*, 014619. [CrossRef]
49. Jokiniemi, L.; Miyagi, T.; Stroberg, S.R.; Holt, J.D.; Kotila, J.; Suhonen, J. Ab initio calculation of muon capture on ^{24}Mg. *Phys. Rev. C* **2023**, *107*, 014327. [CrossRef]
50. Hyvärinen, J.; Suhonen, J. Nuclear matrix elements for $0\nu\beta\beta$ decays with light or heavy Majorana-neutrino exchange. *Phys. Rev. C* **2015**, *91*, 024613. [CrossRef]